For a film with a wavy section ($X_c < 1$) equation (1) becomes

$$\bar{\bar{H}} = 2^{2/3} R_c/3FL + \int_{X_c}^{1} (\bar{\theta}_{0y}/(2R)^{1/3})\,dX \qquad (14)$$

where $\bar{\bar{H}}$ may be estimated provided that values of F, N and L are specified. The integral in equation (14) was estimated by determining X_c and R_c, evaluating the wave number from equation (5), estimating wave amplitude and b from equations (6), (10) and (11), numerically integrating equation (9) for $X > X_c$, and using equation (2) in equation (14).

Int. J. Heat Mass Transfer. Vol. 31, No. 9, pp. 1947–1952, 1988
Printed in Great Britain

0017–9310/88 $3.00 + 0.00

Dynamic instability experiments in a boiling flow system

R. P. Roy and P. Jain

Department of Mechanical and Aerospace Engineering, Arizona State University, Tempe, AZ 85287, U.S.A.

and

S. P. Kalra

Electric Power Research Institute, Palo Alto, CA 94303, U.S.A.

(*Received* 19 *September* 1987 *and in final form* 8 *March* 1988)

INTRODUCTION

Thermally driven flow instabilities in vapor (gas)–liquid flow systems can give rise to major operational problems in various equipment and components of importance. Severe mechanical vibrations and thermal stresses may result from these instabilities. Onset of critical heat flux may also be hastened, leading to burnout of the heated section.

Experimental studies of dynamic instabilities aimed at identifying the instability threshold condition in vapor–liquid flow systems have been numerous (e.g. refs. [1–6]). These studies indicate that the most common dynamic instability is a low frequency (0.1–2 Hz, typically) flow oscillation of the limit cycle type termed density wave oscillations (DWO). Brimley *et al.* [4] made an interesting observation that the onset of instability was frequently not an abrupt phenomenon. Rather, the amplitude of flow oscillations (the test section inlet flow rate was usually the measured variable) increased gradually with increase in heat input. On the other hand, experiments such as ref. [5] reported reasonably clear boundaries across which the flow oscillation amplitude increased sharply.

Our experimental study of a Refrigerant-113 boiling flow system was undertaken as one part of a research effort the goals of which encompassed both theoretical modeling and experiments. The main objective of the experiments was to generate our own data base for validating a dynamic instability model developed in the course of the theoretical effort. One other set of experimental data had been reported earlier for a Refrigerant-113 system [5]. The main difference between our data and those of ref. [5] lies in the geometric configuration of the test section, this being annular with a rather large flow area in our case and tubular in ref. [5].

Our other objective was to visually inspect the subcooled boiling flow field during the inception of flow instability with particular emphasis on the region where significant net vapor generation began. The annular test section with a transparent outer section (pipe) allowed flow visualization as well as flash photography.

EXPERIMENTAL APPARATUS

A schematic diagram of the experimental rig is shown in Fig. 1. The annular test section was oriented vertically, the flow of fluid being upward through it. The outer section of the annulus was comprised of two long segments of transparent pyrex glass pipe (38.1 mm i.d., 47.0 mm o.d.). A 304 stainless steel tube of 15.9 mm o.d. and 1.2 mm wall thickness constituted the inner section of the annulus. The overall test section was 3.66 m long of which heat could be supplied to the upper 2.74 m by resistively heating the inner tube by direct current (the maximum power input possible is 37 kW at present).

Two locations are marked on Fig. 1, namely junctions 1 and 2. These indicate the beginning and the end of our 'test channel', respectively. The annular test section is one part of this test channel, the others being the inlet and exit piping and components. The inlet part contains, in addition to the piping, a preheater (1 kW maximum input power), a turbine flow meter (Flow Technology) and a globe valve which provides a variable inlet flow restriction. The preheater was not operated in these instability experiments since it was important that the entire energy input to the test channel fluid be provided in the test section itself. The exit part contains a ball valve in addition to the piping. This valve provides a variable flow restriction at the test section exit. A differential pressure transducer (Tavis) was used to measure, sequentially, the pressure drops across (i) the inlet piping and components and (ii) the exit ball valve and piping.

A 316 stainless steel centrifugal pump (Ingersol Rand) circulated the fluid through the rig. The pump was capable of providing a flow rate of 570 l min^{-1} (approximately 150 U.S. gpm) at 450 kPa (approximately 65 psi) total dynamic head. Typically, more than 95% of the total pump flow was diverted through a large bypass line (51 mm nominal diameter) installed parallel to the test section.

The following uncertainties apply to the primary measurements made in the course of the instability experiments:

input heating power: ± 10 W
flow rate at test section inlet: $\pm 1 \times 10^{-6}$ m^3 s^{-1}
temperature at test section inlet: ± 0.1 K
system pressure: ± 0.7 kPa.

A dedicated system (DATA 6000, Analogic–Data Precision) equipped with a floppy disk drive and a plotter (Hewlett–Packard) was used to acquire, store and analyze the time series data obtained from the turbine flow meter–monitor.

EXPERIMENTAL PROCEDURE

The variables that nominally described an instability test were: (i) the mean flow rate through the test section, (ii) system pressure and inlet temperature, (iii) inlet and exit flow

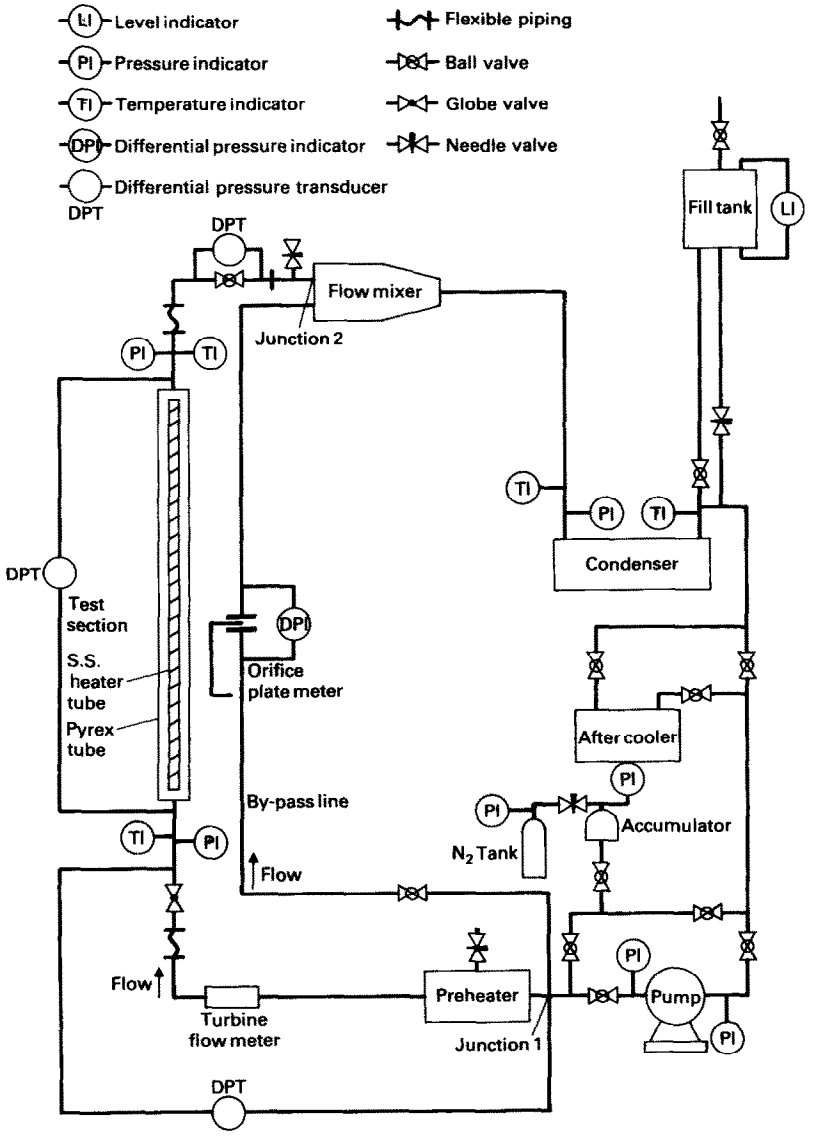

FIG. 1. A schematic diagram of the experimental rig.

restrictions (in terms of the respective coefficients, K_i and K_c)† and (iv) the heating power input to the test section.

Points (i) through (iii) were established at the beginning of each instability experiment. Heating power was then applied to the test section in small quasistatic steps. Intermittently, small reductions in the cooling water supply to the main heat exchanger were made, this being the most effective means of increasing the fluid temperature at the test section inlet. The final approach to the instability threshold was via very small quasistatic increases in the heat input. The mean, r.m.s. and peak-to-peak values of the test section inlet flow rate (based on the turbine flow meter measurement) was continuously monitored by the data acquisition system. The instability threshold was considered to be reached when sustained oscillation of a recognizable amplitude was detected in the inlet flow rate. Upon establishment of sustained flow oscillations of recognizable amplitude, time series data of the inlet flow rate was recorded (typically, 2560 sample points with a sampling interval of 100 ms). The auto power spectral density function of this data was constructed to obtain the instability frequencies.

Some difficulty was encountered in many of our experiments in clearly establishing the instability threshold condition by the criterion that the flow oscillation amplitude would increase from a very small value to a significantly large value across this boundary. Instead, both the peak-to-peak variation of the flow rate and its r.m.s value exhibited gradual, and often ramp-like, increases in response to increases in the heat input when the system was close to the instability threshold. This is similar to the observation of Brimley *et al.* [4] mentioned earlier. In our experiments, this may have been caused by the large flow area of the test section and the correspondingly large fluid inertia.

RESULTS

Table 1 shows the instability threshold results for the experiments conducted at a system pressure of 269.7 kPa. Results for the experiments at a system pressure of 325.0 kPa are presented in Table 2. For each experiment, the mean

† The flow restriction coefficient is defined as $(\Delta p/\frac{1}{2}\rho u^2)$, where u is the bulk velocity.

Table 1. Flow instability experimental results and comparison with theoretical model predictions for a system pressure of 269.7 kPa

		Inlet restriction		Outlet restriction			Experimental result		Model prediction	
Experiment No.	Test channel inlet flow rate ($m^3 s^{-1} \times 10^4$)	Mean ΔP across the preheater inlet and the test channel inlet globe valve exit (kPa)	Inlet restriction coefficient, K_i	Mean ΔP across the test channel outlet ball valve (kPa)	Outlet restriction coefficient, K_e	Test channel inlet temperature (K)	Input power (at the inner surface of the annular channel) (kW)	Flow instability frequencies (in decreasing order of energy content) (Hz)	Input heating power (kW)	Flow instability frequencies (Hz)
8E	2.64	21.04	177.0	36.60	101.0	328.0	9.71	0.390, 0.117	9.99	0.292, 0.061
10A	3.29	26.17	143.0	22.76	53.0	331.5	10.01	0.556, 0.185 0.048	9.91	0.349
11H	2.99	11.91	78.0	39.87	127.0	329.5	7.10	0.273, 0.586	7.26	0.353, 0.071
12A	3.18	17.99	108.0	34.02	91.8	328.6	8.06	0.469, 0.273	8.54	0.364, 0.075
13A	2.69	14.88	122.0	38.43	136.0	327.5	7.70	0.273, 0.39 0.507	8.08	0.313, 0.061
14A	2.62	14.28	123.0	41.50	139.0	325.4	8.80	0.351, 0.234 0.078	9.12	0.307, 0.057
15A	2.65	19.13	161.5	39.13	111.0	325.0	10.30	0.585, 0.390 0.273, 0.156 0.078	10.25	0.305, 0.06

Table 2. Flow instability experimental results and comparison with theoretical model predictions for a system pressure of 325.0 kPa

		Inlet restriction		Outlet restriction			Experimental result		Model prediction	
Experiment No.	Test channel inlet flow rate ($m^3 s^{-1} \times 10^4$)	Mean ΔP across the preheater inlet and the test channel inlet globe valve exit (kPa)	Inlet restriction coefficient, K_i	Mean ΔP across the test channel outlet ball valve (kPa)	Outlet restriction coefficient, K_e	Test channel inlet temperature (K)	Input power (at the inner surface of the annular channel) (kW)	Flow instability frequencies (in decreasing order of energy content) (Hz)	Input heating power (kW)	Flow instability frequencies (Hz)
20A	2.77	18.03	141.0	37.64	111.0	333.7	9.83	0.273, 0.625 0.078, 0.781 0.390	9.83	0.313, 0.065
21A	2.73	22.13	178.0	34.11	89.5	333.3	11.16	0.313, 0.195	11.06	0.307
22A	2.70	12.99	106.5	40.87	139.0	333.0	9.02	0.507, 0.117 0.312	9.14	0.313, 0.065
23A	3.00	19.95	134.0	35.56	80.0	336.0	11.03	0.390, 0.195 0.117	10.59	0.329, 0.074
24A	3.07	16.17	103.0	37.49	94.0	334.7	9.95	0.117, 0.429 0.313, 0.547	9.49	0.349, 0.077
25A	3.14	12.69	77.5	38.78	106.0	335.1	8.71	0.273, 0.469 0.195	9.05	0.358, 0.078
26B	3.11	17.13	107.0	35.60	97.0	337.7	8.49	0.313, 0.156 0.547, 0.390 0.664	8.80	0.342, 0.076

test section flow rate, inlet liquid temperature, input heating power and the flow instability frequencies (in decreasing order of their energy content) are reported corresponding to the condition just beyond the instability threshold.

A mismatch, small, but found to be important to the dynamic instability model, was detected between our visually observed NVG location and the one predicted by the Saha–Zuber criterion [5] in almost all our experiments. A small modification was therefore incorporated in the criterion. This is briefly discussed in the Appendix.

COMPARISON WITH THEORETICAL MODEL PREDICTIONS

The governing and constitutive equations of the theoretical model as well as the steady state and linear stability solution methodologies have already been presented elsewhere [7]. Therefore, they have been omitted from this note with the exception of the net vapor generation criterion which is briefly discussed in the Appendix.

Tables 1 and 2 also show comparisons of the model predictions of the instability threshold with the experimental data. The model calculations are based on a 26-cell representation of the test channel, the results having been found invariant for a number of cells larger than 26.

Agreement *vis-à-vis* the threshold input heating power is quite good. On the other hand, the model usually predicts a single oscillatory instability frequency whereas the experiments yielded multiple frequencies with one being dominant.† In some cases two instability frequencies are predicted by the model (e.g. Experiments 13A, 14A, 20A and 22A).

DISCUSSION

As evident from the experimental conditions given in Tables 1 and 2 all of our experiments were run at rather high subcooling at the test section inlet. This is a limitation which was brought about by an insufficient provision for axial thermal expansion of the test section heater tube during conditions at which high inlet liquid temperature and high input heating power coexisted. Given this, only a limited experimental study of the parametric effects on the instability boundary could be carried out. One such study (e.g. Experiments 14A and 15A) showed that increasing the inlet flow restrictions (K_i) has a stabilizing influence which, of course, is a well-known effect. Another (e.g. Experiments 8E and 21A) demonstrated that increasing the system pressure has a stabilizing influence on the system. This is also in agreement with the findings of other investigators.

As pointed out earlier, multiple instability frequencies were detected in the experiments although a dominant frequency was always found. We note, however, that the cumulative amount of energy associated with the non-dominant frequencies was not trivial, amounting typically to about one-third of the total flow oscillation energy (i.e. the mean square value of the oscillation). The linear stability analysis, on the other hand, usually predicted a single dominant frequency although it did predict two frequencies in some cases. Two reasons can be offered for this apparent discrepancy. One is that certain phenomena (e.g. pump-generated pulsations, perturbations generated by boiling flow through valves, mixing and condensation in the flow mixer, etc.) were not accounted for by the theoretical model but must have caused disturbances in the actual system. The other reason is that linear analysis cannot predict the additional oscillation modes (harmonics, etc.) which may appear at finite amplitudes (i.e. in the non-linear region).

† By the term 'dominant frequency' we mean that the amount of energy contained in this oscillatory mode of the overall instability is the largest by a significant margin.

Acknowledgement—This work was supported by Electric Power Research Institute, Nuclear Power Division, under research project RP495-2.

REFERENCES

1. A. H. Stenning and T. N. Veziroglu, Flow oscillation models in forced convection boiling, *Proc. 1965 Heat Transfer and Fluid Mechanics Institute*, pp. 301–316. Stanford University Press, Stanford, California (1965).
2. L. G. Neal, S. M. Zivi and R. W. Wright, The mechanism of hydrodynamic instabilities in boiling flow systems, *Proc. Symp. on Two-phase Flow Dynamics*, Eindhoven (1967).
3. G. Yadigaroglu and A. E. Bergles, Fundamentals and higher-mode density-wave oscillations in two-phase flow, *ASME J. Heat Transfer* **94,** 189–195 (1972).
4. W. Brimley, W. B. Nicoll and A. B. Strong, Flow oscillations in fixed-pressure-drop flow boiling systems with random excitation, *Int. J. Heat Mass Transfer* **19,** 1379–1386 (1976).
5. P. Saha, M. Ishii and N. Zuber, An experimental investigation of the thermally induced flow oscillations in two-phase systems, *ASME J. Heat Transfer* **94,** 616–622 (1976).
6. D. M. France, R. D. Carlson and R. P. Roy, Measurement and analysis of dynamic instabilities in fluid heated two-phase flow, *Int. J Heat Mass Transfer* **29,** 1919–1929 (1986).
7. R. C. Dykhizen, R. P. Roy and S. P. Kalra, A linear time-domain two-fluid model analysis of dynamics instability in boiling flow system, *ASME J. Heat Transfer* **108,** 100–108 (1986).
8. S. Z. Rouhani, Void measurements in the regions of subcooled and low-quality boiling, Report No. AE-RTL-849 (1966).
9. R. Evangelisti and P. Lupoli, The void fraction in an annular channel at atmospheric pressure, *Int. J. Heat Mass Transfer* **12,** 699 (1969).
10. G. E. Dix, Vapor void fractions for forced convection with subcooled boiling at low flow rate, Ph.D. Thesis, University of California, Berkeley. Also General Electric Report NEDO-10491 (1971).

APPENDIX: THE NET VAPOR GENERATION LOCATION

The net vapor generation (NVG) criterion of Saha *et al.* [5] was modified slightly to reflect our visual observation of the subcooled boiling region. Since, in all our experiments, the Peclet number (Pe) was large ($>10^5$), NVG may be regarded as hydrodynamically controlled. Therefore, only the second part of the two-part criterion [5], which is for $Pe > 70\,000$, would apply. The modification suggested in the following should then only be considered for such high Peclet numbers.

The need for this modification appears to have been brought about by the combined effects of the channel geometry (annular) and dimensions resulting in large relative spacing between inner and outer walls $(R_o - R_i)/R_i$. Data from three previous annular geometry experimental studies [8–10] had been considered during the development of the Saha–Zuber criterion. However, the relative spacings between the walls in those annuli (equal to 1.083, 0.857, and 0.962, respectively) were not nearly as large as ours (equal to 1.399).

It is easily shown that the original two-part criterion can be consolidated without causing any change in the liquid subcooling prediction in either Peclet number range to

$$(\Delta T_{sub})_{NVG} = \frac{q''_w}{[(455k_L/D_h)X + (0.0065GC_p)Y]} \quad \text{(A1)}$$

Table A1

Annular channel With heat input at inner wall	Annular channel With heat input at outer wall	Hydraulically equivalent circular channel
$q''_{ACi} = \frac{q'_w}{2\pi R_i}$	$q''_{ACo} = \frac{q'_w}{2\pi R_o}$	$q''_{ECC} = \frac{q'_w}{2\pi(R_o - R_i)}$

where

$$X = 1 - \exp(-0.48 \times 10^5/Pe)$$

and

$$Y = 1 - \exp(-0.98 \times 10^{-5}/Pe).$$

That this criterion is valid for tubular channels of various sizes is borne out to a certain extent by the size range considered in the development of the criterion. Let us now replace the annular channel by a hydraulically equivalent tubular channel of diameter $2(R_o - R_i)$. Keeping the heat input rate per unit channel length, q'_w, the same, Table A1 gives the situations *vis-à-vis* wall heat flux. Therefore

$$\frac{q''_{ACi}}{q''_{ECC}} = \frac{R_o - R_i}{R_i} = \gamma_i$$

and

$$\frac{q''_{ACo}}{q''_{ECC}} = \frac{R_o - R_i}{R_o} = \gamma_o.$$

We propose that the wall heat flux, q''_w, which appears in equation (A1) be replaced by q''_{wECC}. Note that if the test section is tubular, q''_{wECC} is the actual wall heat flux imposed and equation (A1) remains the same. It, however, is modified in the case of annular geometry

$$(\Delta T_{sub})_{NVG} = \frac{q''_{wECC}}{[(455k_L/D_h)X + (0.0065GC_p)Y]} = \frac{q''_{wACj}}{\gamma_j[(455k_L/D_h)X + (0.0065GC_p)Y]} \quad (A2)$$

where j = i or o.

Note that $\gamma_j > 1$ causes the predicted NVG location to move downstream in the channel (with respect to the location where heating begins) provided NVG does not occur at the beginning of the heating in both cases. On the other hand, $\gamma_j < 1$ causes the predicted NVG location to move upstream.

The preceding modification suggested for high Peclet number ($\approx 10^5$ or higher) flows is tentative since its verification is rather limited. However, it appears to be reasonable to propose that $\gamma_j (j$ = i or o) be adopted as the upper or lower (as appropriate) limit of a correction parameter β_j such that

$$1 \leqslant \beta_i \leqslant \gamma_i \quad (\text{if } \gamma_i > 1)$$

$$\gamma_i \leqslant \beta_i \leqslant 1 \quad (\text{if } \gamma_i < 1)$$

and

$$1 \geqslant \beta_o \geqslant \gamma_o.$$

The optimum value of β_j (within the above ranges) for a particular annular channel should be decided upon by flow visualization when feasible. When this is not possible, indirect optimization via comparison of modal-calculated axial vapor fraction profiles with corresponding experimental data could be used. For our test section, we estimated the following value of β_i to be suitable on the basis of flow visualization:

$$\beta_i = 1.25 \pm 0.05.$$

In the calculational result of Tables 1 and 2, $\beta_i = 1.25$ has been used.

Int. J. Heat Mass Transfer. Vol. 31, No. 9, pp. 1952–1954, 1988
Printed in Great Britain

0017–9310/88 $3.00 + 0.00
Pergamon Press plc

The use of the Walsh functions for the study of periodic diffusive phenomena in a multilayer medium

G. GUIFFANT, A. ARHALIASS and J. DUFAUX
L.B.H.P., Université Paris 7, 2 place Jussieu, 75251 Paris Cedex 05, France

(*Received* 3 *December* 1987)

INTRODUCTION

A VERY simple method for studying transient diffusive phenomena in multilayer media was proposed by Gosse [1]. This approach is extended to periodic external conditions by using developments on an orthogonal complete base of rectangular functions called 'Walsh functions'. We take advantage of this note to emphasize the interest of the problem both for practical applications and for the methods used. The study of the transport phenomena in the microcirculation is then pointed out as a particular example of the possible transfer of methods by means of analogies.

The main features of the transient diffusive phenomena in heterogeneous media are both dependent on the nature of the constitutive materials and on their geometrical repartition. Thus, two classes of media can be taken into consideration: (a) composite materials which are constituted of a solid dispersed phase of regular or irregular shape elements; (b) media made up of successive ajoining layers of different materials.

Owing to the possible applications, the study of the diffusion in multilayer media occurs in situations where the system is submitted (at least on one external face) to periodic limiting conditions: as an example, in the field of thermal study, we use here as a point of reference, the alternate watch and fire temperature or the day–night succession (thermal analysis of stratified soils, thermal energy storage, isolating walls, etc.).

According to the preceding statement, the problem gives the opportunity to develop methods of resolution allowing, by means of analogies, to start on any other question defined in a similar way. From this point of view, the development of models for the study of transport phenomena in the microcirculation is mentioned here [2]. In the microvascular bed, blood flow is mainly controlled by viscous forces. Thus, it can be shown [3] that the intravascular pressure is a solution of a diffusion equation with a diffusivity as a function of the blood viscosity and characteristic parameters of the vessel: dimensions and Young's modulus. The observation *in situ* of microcirculatory networks (double tree vascularization of vessels with decreasing and increasing diameters) leads to postulate [3] a representation consisting of a number of levels connected in series, each level being characterized by constant and uniform parameters (same geometric parameters, viscosity and Young's modulus). Moreover, the equation for the blood flow continuity between two levels [3] is analogous